
Sourcerer: Sample-based Maximum Entropy Source Distribution Estimation

Julius Vetter^{†,1,2,*}Guy Moss^{†,1,2,*}Cornelius Schröder^{1,2}Richard Gao^{1,2}Jakob H. Macke^{1,2,3,*}¹Machine Learning in Science, Excellence Cluster Machine Learning, University of Tübingen²Tübingen AI Center³Department Empirical Inference, Max Planck Institute for Intelligent Systems
Tübingen, Germany[†]Equal contribution.

Abstract

Scientific modeling applications often require estimating a distribution of parameters consistent with a dataset of observations—an inference task also known as source distribution estimation. This problem can be ill-posed, however, since many different source distributions might produce the same distribution of data-consistent simulations. To make a principled choice among many equally valid sources, we propose an approach which targets the maximum entropy distribution, i.e., prioritizes retaining as much uncertainty as possible. Our method is purely sample-based—leveraging the Sliced-Wasserstein distance to measure the discrepancy between the dataset and simulations—and thus suitable for simulators with intractable likelihoods. We benchmark our method on several tasks, and show that it can recover source distributions with substantially higher entropy than recent source estimation methods, without sacrificing the fidelity of the simulations. Finally, to demonstrate the utility of our approach, we infer source distributions for parameters of the Hodgkin-Huxley model from experimental datasets with thousands of single-neuron measurements. In summary, we propose a principled method for inferring source distributions of scientific simulator parameters while retaining as much uncertainty as possible.

1 Introduction

In many scientific and engineering disciplines, mathematical and computational simulators are used to gain mechanistic insights. A common challenge is to identify parameter settings of such simulators that make their outputs compatible with a set of empirical observations. For example, by finding a distribution of parameters that, when passed through the simulator, produces a distribution of outputs that matches that of the empirical dataset of observations.

Suppose we have a stochastic simulator with input parameters θ and output x , which allows us to generate samples from the forward model $p(x|\theta)$ (which is usually intractable). We have acquired a dataset $\mathcal{D} = \{x_1, \dots, x_n\}$ of observations with empirical distribution $p_o(x)$, and want to identify

*{firstname.secondname}@uni-tuebingen.de

a distribution $q(\theta)$ over parameters that, once passed through the simulator, yields a “pushforward” distribution of simulations $q^\#(x) = \int p(x|\theta)q(\theta)d\theta$ that is indistinguishable from the empirical distribution. This setting is known by different names in different disciplines, for example as *unfolding* in high energy physics [8], *population of models* in electrophysiology [26] and *population inference* in gravitational wave astronomy [49]. Adopting the terminology of Vandegar et al. [52], we refer to this task as *source distribution estimation*.

A common approach to source distribution estimation is empirical Bayes [45, 13]. Empirical Bayes uses hierarchical models in which each observation is modeled as arising from different parameters $p(x_i|\theta_i)$. The hyper-parameters of the prior (and thus the source q_ϕ) are found by optimizing the marginal likelihood $p(D) = \prod_i \int p(x_i|\theta)q_\phi(\theta)d\theta$ over ϕ . Empirical Bayes has been successfully applied to a range of applications [27, 28, 49]. However, empirical Bayes is typically not applicable to models with intractable likelihoods, which is usually the case for scientific simulators. Using surrogate models for such likelihoods, empirical Bayes has been extended to increasingly more complicated parameterizations ϕ of the source distribution, including neural networks [53, 52].

A more general issue, however, is that the source distribution problem can often be ill-posed without the introduction of a hyper-prior or other regularization principles, as also noted in Vandegar et al. [52]: Distinct source distributions $q(\theta)$ can give rise to the same data distribution $q^\#(x)$ when pushed through the simulator $p(x|\theta)$ (Fig. 1, illustrative example in Appendix A.6).

In this work, we use the maximum entropy principle, i.e., to choose the “maximum ignorance” distribution within a class of distributions to resolve the ill-posedness of the source distribution problem [17, 21]. The maximum entropy principle formalizes the notion that the optimal choice for distributions should “assume less”. It has been applied to specific source distribution estimation problems in scientific disciplines such as cosmology [20] and high-energy physics [8].

Our contributions We introduce *Sourcerer*², a general method for source distribution estimation for simulators, providing two key innovations: First, we target the maximum entropy source distribution to obtain a well-posed problem, thereby increasing the entropy of the estimated source distributions at no cost to their fidelity. Second, we use general distance metrics between distributions such as the Sliced-Wasserstein distance, instead of maximizing the marginal likelihood as in empirical Bayes. This allows evaluation of the objective using *only samples*, removing the requirement to have simulators or surrogate models with a tractable likelihood. We validate our method on multiple tasks, including tasks with high-dimensional observation space, which are challenging for likelihood-based methods. Finally, we apply our method to estimate the source distribution over the mechanistic parameters of the Hodgkin-Huxley model from a large (~ 1000 samples) dataset of electrophysiological recordings.

2 Methods

We formulate the source distribution estimation problem in terms of the maximum entropy principle. The (differential) entropy $H(p)$ of a distribution $p(\theta)$ is defined as

$$H(p) = - \int p(\theta) \log p(\theta) d\theta. \quad (1)$$

²Code available at <https://github.com/mackelab/sourcerer>

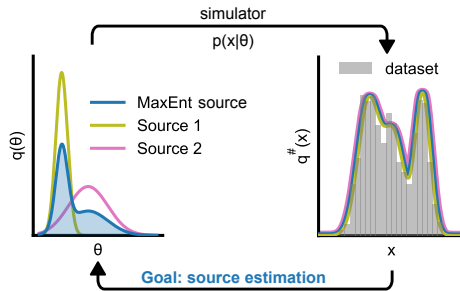


Figure 1: **Maximum entropy source distribution estimation.** Given an observed dataset $\mathcal{D} = \{x_1, \dots, x_n\}$ from some data distribution $p_o(x)$, the *source distribution estimation* problem is to find the parameter distribution $q(\theta)$ that reproduces $p_o(x)$ when passed through the simulator $p(x|\theta)$, i.e. $q^\#(x) = \int p(x|\theta)q(\theta)d\theta = p_o(x)$. This problem can be ill-posed, as there might be more than one distinct source distribution. We resolve this by targeting the maximum entropy distribution, which is unique.

2.1 Data-consistency and regularized objective

For a given distribution $q(\theta)$ and simulator with (possibly intractable) likelihood $p(x|\theta)$, the *push-forward* of q is given by $q^\#(x) = \int p(x|\theta)q(\theta)d\theta$. The distribution q is a source distribution if its pushforward matches the observed data distribution $p_o(x)$, that is, $q^\# = p_o$ almost everywhere. Equivalently, given a distance metric $D(\cdot, \cdot)$ between probability distributions $P(\mathcal{X})$ over the data space \mathcal{X} , a source distribution q is one which satisfies $D(q^\#, p_o) = 0$. In general, for a given distribution of observations $p_o(x)$ and likelihood $p(x|\theta)$, the source distribution problem is ill-posed as there are possibly many different source distributions. The maximum entropy principle can be employed to resolve this ill-posedness:

Proposition 2.1. *Let $Q = \{q|q^\# = p_o\}$ be the set of source distributions for a given likelihood $p(x|\theta)$ and data distribution p_o . Suppose that Q is non-empty and compact. Then $q^* = \arg \max_{q \in Q} H(q)$ exists and is unique.*

This proposition follows from the fact that the set of source distributions is convex and that the (differential) entropy $H(q)$ is a strictly concave functional. See Appendix A.6 for a proof and additional assumptions.

Proposition 2.1 suggests to solve the constrained optimization problem

$$\max_{\phi} H(q_{\phi}) \quad \text{s.t.} \quad D(q_{\phi}^\#, p_o) = 0, \quad (2)$$

where q_{ϕ} is some parametric family of distributions.

Practically, however, a solution might not exist, for example due to simulator misspecification. Furthermore, even if a solution exists, it is difficult to obtain since we only have a fixed number of samples from p_o and can only estimate $D(q_{\phi}^\#, p_o)$. We therefore propose a *regularized* version of Eq. (2) and solve

$$\max_{\phi} \lambda H(q_{\phi}) - (1 - \lambda) \log(D(q_{\phi}^\#, p_o)) \quad (3)$$

instead, where λ is a parameter determining the strength of the data-consistency term and the logarithm is added for numerical stability. This regularized objective is related to the Lagrangian relaxation of Eq. 2, where now $\log D(q^\#, p_o) \leq \log \epsilon$ for some $\epsilon > 0$ and the dual variable is $(1 - \lambda)/\lambda$.

For $\lambda \rightarrow 1$, the loss in Eq. 3 is dominated by the entropy term, and for $\lambda \rightarrow 0$ by the data-consistency term. We apply ideas from constrained optimization and reinforcement learning [42, 4, 1] and use a dynamical schedule during training. We initialize training with $\lambda_{t=1} = 1$, and decay this value linearly to a terminal value $\lambda_{t=T} = \lambda > 0$ over the course of training. This dynamical schedule encourages the variational source model to first explore high-entropy distributions, and later increase consistency with the data between high-entropy distributions. Pseudocode and details of the schedule in Appendix A.2.

2.2 Reference distribution

For many tasks, there is an additional constraint in terms of a reference distribution $p(\theta)$. For example, in the Bayesian inference framework, it is common to have a prior distribution $p(\theta)$, encoding existing knowledge about the parameters θ from previous studies. In such cases, a distribution with higher entropy than $p(\theta)$, even if it is a source distribution, is not always desirable. We therefore adapt our objective function in Eq. (3) to minimize the Kullback-Leibler (KL) divergence between the source $q(\theta)$ and the reference $p(\theta)$:

$$\min_{\phi} \lambda D_{KL}(q||p) + (1 - \lambda) \log(D(q^\#, p_o)). \quad (4)$$

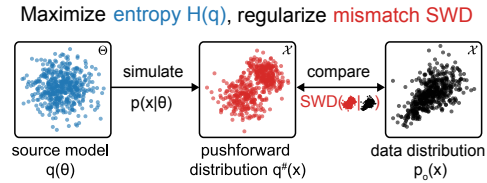


Figure 2: **Overview of Sourcerer.** Given a source distribution $q(\theta)$, we sample $\theta \sim q$ and simulate using $p(x|\theta)$ to obtain the pushforward distribution $q^\#(x) = \int p(x|\theta)q(\theta)d\theta$. We maximize the entropy of the source distribution $q(\theta)$ while regularizing with a Sliced-Wasserstein distance (SWD) term between the pushforward of $q^\#$ and the data distribution $p_o(x)$ (Eq. 3). Θ and \mathcal{X} in top right corner of boxes denote parameter space and data/observation space, respectively.

The KL divergence term can be rewritten as $D_{KL}(q||p) = -H(q) + H(q, p)$, where $H(q, p) = -\int \log(p(\theta))q(\theta)d\theta$ is the cross-entropy between q and p . Thus, provided we can evaluate the density $p(\theta)$, we can obtain a sample-based estimate of the loss in Eq. (4). In our work, we consider $p(\theta)$ to be the uniform distribution over some bounded domain B_Θ (and hence the maximum entropy distribution on this domain). This ‘‘box prior’’ is often used as the naive estimate from literature observations in inference studies. More specifically, in this case, $H(q, p) = -1/|B_\Theta|$, where $|B_\Theta|$ is the volume of B_Θ . Therefore, it is independent of q , and hence minimizing the KL divergence is equivalent to maximizing $H(q)$ on B_Θ . In the case where $p(\theta)$ is non-uniform (e.g., Gaussian) the cross-entropy term regularizes the loss by penalizing large $q(\theta)$ when $p(\theta)$ is small.

2.3 Sliced-Wasserstein as a distance metric

We are free to choose any distance metric $D(\cdot, \cdot)$ for the loss function Eq. (4). In this work, we use the fast, sample-based, and differentiable Sliced-Wasserstein distance (SWD) [6, 23, 37] of order 2. The SWD is defined as the expected value of the 1-dimensional Wasserstein distance between the projections of the distribution onto uniformly random directions u on the unit sphere \mathbb{S}^{d-1} in \mathbb{R}^d . More precisely, SWD is defined as

$$\text{SWD}_m(p, q) = \mathbb{E}_{u \sim \mathcal{U}(\mathbb{S}^{d-1})} [W_m(p_u, q_u)], \quad (5)$$

where p_u is the 1-dimensional distribution with samples $u^\top x$ for $x \sim p(x)$, and W_m is the 1-dimensional Wasserstein distance of order m . In the empirical setting, where we are given n samples each from p_u and q_u respectively, the 1-dimensional Wasserstein distance is computed from the order statistics as

$$W_m(p_u, q_u) = \left(\sum_{i=1}^n \|x_p^{(i)} - x_q^{(i)}\|_m^m \right)^{1/m}, \quad (6)$$

where $x_p^{(i)}$ denotes the i -th order statistic of the samples from p_u (and similarly for $x_q^{(i)}$), and $\|\cdot\|_m$ denotes the L^m distance on \mathbb{R} . The sample-based 1-dimensional Wasserstein distance can thus be computed in $\mathcal{O}(n \log n)$ time in the number of datapoints n [6], which is significantly faster than computing the multi-dimensional Wasserstein distance ($\mathcal{O}(n^3)$, 25). While the SWD is not the same as the multi-dimensional Wasserstein distance, it is still a valid metric on the space of probability distributions [37].

2.4 Differentiable simulators and surrogates

To regress on the loss in Eq. 3, we only require that sampling from the simulator $p(x|\theta)$ is a differentiable operation. This is a distinct requirement from likelihood-based approaches such as Vandegar et al. [52], which require that the likelihood $p(x|\theta)$ can be evaluated explicitly *and* differentially. This means that our sample-based approach can be readily applied to a larger set of simulators than likelihood-based approaches.

In practice, however, many simulators do not satisfy either condition; they are not differentiable, and the likelihood can not be evaluated explicitly. For such simulators, we first train a surrogate model. Sample-based approaches can make use of surrogates that model the likelihood only implicitly. Such surrogate models can be easier to train and evaluate in practice.

2.5 Source Model

In this work we use neural samplers as proposed in Vandegar et al. [52] to parameterize a source model q_ϕ . These samplers employ unconstrained neural network architectures (in our case a multi-layer perceptron) to transform a random sample from $z \in \mathcal{N}(0, I)$ into a sample from q_ϕ . While neural samplers do not have a tractable likelihood, they are faster to evaluate than models with tractable likelihoods. Furthermore, by using unconstrained network architectures, neural samplers are flexible and additional constraints (e.g., symmetry, monotonicity) are easily introduced.

To use likelihood-free source parameterizations, we require a purely sample-based estimator for the entropy $H(q_\phi)$. This can be done using the *Kozachenko-Leonenko* entropy estimator [24, 3], which is based on a nearest-neighbor density estimate. We use the Kozachenko-Leonenko estimator in this work for its simplicity, but note that sample-based entropy estimation is an active area of research, and other choices are possible [41]. Details in Appendix A.5.

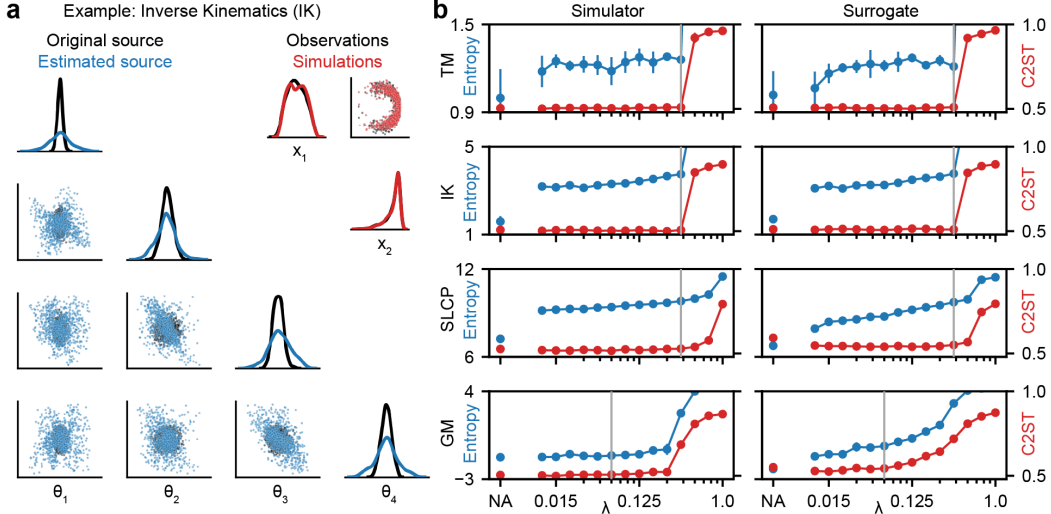


Figure 3: **Results for the source estimation benchmark.** (a) Original and estimated source and corresponding pushforward for the differentiable IK simulator ($\lambda = 0.35$). The estimated source has higher entropy than the original source that was used to generate the data. The observations (simulated with parameters from the original source) and simulations (simulated with parameters from the estimated source) match. (b) Performance of our approach for all four benchmark tasks (TM, IK, SLCP, GM) using both the original, differentiable simulators, and learned surrogates. Source estimation is performed without (NA) and with entropy regularization for different choices of λ . For all cases, mean C2ST accuracy between observations and simulations (lower is better) as well as the mean entropy of estimated sources (higher is better) over five runs are shown together with the standard deviation. The gray line at $\lambda = 0.35$ ($\lambda = 0.062$ for GM) indicates our choice of terminal λ for the numerical benchmark results (Table 1).

3 Experiments

To evaluate the data-consistency and entropy of source distributions estimated by Sourcerer, we benchmark our method against Neural Empirical Bayes (NEB) [52], a state-of-the-art approach to source distribution estimation. The benchmark comparison is performed on four source distribution estimation tasks including three presented in Vandegar et al. [52]. We then demonstrate the advantage of Sourcerer in the case of differentiable simulators with a high-dimensional data domain, where likelihood-based empirical Bayes approaches would require training a likelihood surrogate. Finally, we use Sourcerer to estimate the source distribution for a Hodgkin-Huxley simulator of single-neuron voltage dynamics from a large dataset of real electrophysiological recordings.

3.1 Source Estimation Benchmark

Benchmark tasks The source estimation benchmark contains four simulators: two moons (TM), inverse kinematics (IK), simple likelihood complex posterior (SLCP), and Gaussian Mixture (GM) (details about simulators and source distributions are in Appendix A.1). Notably, all four simulators are differentiable. Therefore, we can evaluate our method directly on the simulator as well as trained surrogates. For all four simulators, source estimation is performed on a synthetic dataset of 10000 observations that were generated by sampling from the original source distribution and evaluating the resulting pushforward distribution using the corresponding simulator. The quality of the estimated source distributions is measured using a classifier two sample test (C2ST) [29] between the observations and simulations from the source. We also report the entropy of the estimated sources. Given two sources with the same C2ST accuracy, the higher entropy source is preferable. We compare to the NEB estimator with the same MLP parameterization of the source model and 1024 Monte Carlo samples to estimate the marginal likelihood (details in Appendix A.2).

Table 1: **Numerical benchmark results for Sourcerer.** We show the mean and standard deviation over 5 runs for differentiable simulators and surrogates of Sourcerer on the benchmark tasks, and compare to NEB. All approaches achieve C2ST accuracies close to 50%. For the Sliced-Wasserstein-based approach, the entropies of the estimated sources are substantially higher (bold) with the entropy regularization ($\lambda = 0.35$ for TM, IK, SLCP, $\lambda = 0.062$ for GM, gray line in Fig. 3). They are also higher than the entropy of the sources estimated by NEB.

Task	Two Moons		Inverse Kinematics		SLCP		Gaussian Mixture	
	C2ST acc.	Entropy	C2ST acc.	Entropy	C2ST acc.	Entropy	C2ST acc.	Entropy
Sim. (w/o reg.)	0.5 (0.008)	1.0 (0.198)	0.51 (0.005)	1.59 (0.246)	0.53 (0.006)	7.23 (0.052)	0.5 (0.006)	-1.25 (0.106)
Sim. (with reg.)	0.51 (0.004)	1.26 (0.022)	0.51 (0.002)	3.75 (0.066)	0.53 (0.005)	9.81 (0.039)	0.51 (0.005)	-1.12 (0.083)
Sur. (w/o reg.)	0.51 (0.006)	1.02 (0.162)	0.51 (0.01)	1.7 (0.165)	0.59 (0.017)	6.76 (0.302)	0.55 (0.005)	-2.19 (0.212)
Sur. (with reg.)	0.51 (0.003)	1.21 (0.054)	0.51 (0.005)	3.78 (0.022)	0.55 (0.003)	9.74 (0.039)	0.54 (0.006)	-0.36 (0.095)
NEB	0.53 (0.005)	1.13 (0.093)	0.6 (0.014)	0.82 (0.712)	0.53 (0.006)	7.56 (0.097)	0.52 (0.004)	-1.5 (0.052)

Benchmark performance We first check whether minimizing the Sliced-Wasserstein distance, instead of maximizing the NEB objective of marginal likelihood, finds good source distributions. This corresponds to the case $\lambda = 0$ in Eq. 3 without any decay. We find that for the differentiable simulators, the Sliced-Wasserstein-based approach is able to find good source distributions with C2ST accuracies close to 50% for all benchmark tasks (Fig. 3, labeled NA). This also applies when we use surrogate models to generate the pushforward distributions. In particular, the quality of the estimated source distributions matches those found by NEB (Table 1).

We apply entropy regularization as defined in 3 for all benchmark tasks. The entropy of the estimated sources is drastically increased *without* any cost in the quality of the simulations (Fig. 3b). While C2ST accuracy remains close to 50% across all benchmark tasks, the entropy of estimated sources is substantially higher than that of sources estimated with NEB, or when minimizing only the SWD term (Table 1). We also explore the dependence of the results on the terminal regularization strength λ (Fig. 3b). We observe a sharp trade-off: above a critical value of λ , the SWD term becomes too weak, and the fidelity of the simulations rapidly declines. However, below this critical value of λ , the estimated sources produce simulations that match the observations, and have comparable entropy.

Additionally, for both IK and SLCP simulators, the entropy of the sources estimated by our method is higher than the entropy of the original source distribution (Fig. 3a and Appendix A.9) despite the simulations and observations being indistinguishable from each other (C2ST accuracy: 50%). This does not contradict our approach: The original source distribution just happens not to be the maximum entropy source for these simulators.

3.2 Differentiable Simulators: Lotka-Volterra and SIR

Since our method is sample-based and does not require likelihoods, it is possible to estimate sources by back-propagating through the differentiable simulators directly, instead of first training a surrogate likelihood model, which can be challenging when faced with high-dimensional data such as time series. Here, we highlight this capability by estimating source distributions for two high-dimensional simulators, the Lotka-Volterra model and the SIR (Susceptible, Infectious, Recovered) model. The Lotka-Volterra model is used to model the density of two populations, predators and prey. The SIR model is commonly used in epidemiology to model the spread of disease in a population (details about both models and source distributions in Appendix A.1). Compared to the benchmark tasks in Sec. 3.1, the dimensionality of the data space is much larger: Both the Lotka-Volterra and the SIR model are simulated for 50 time points resulting in a 100 and 50 dimensional time series, respectively.

Furthermore, to show that unlike NEB (which maximizes the marginal likelihood), our sample-based approach can deal with deterministic simulators, we use a deterministic version of the SIR model with no observation noise. Similarly to the benchmark tasks, we define a source, and simulate 10000 observations using samples from this source to define a synthetic dataset on which to perform source distribution estimation. Here, we directly evaluate the quality of the estimated source distributions using the Sliced-Wasserstein distance (see Appendix A.9 for C2ST accuracies). We compare this distance to the minimum distance, which is the distance between simulations of different sets of samples from the same original source.

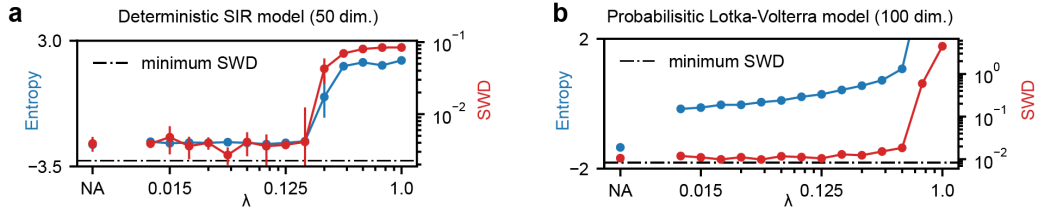


Figure 4: **Source estimation on differentiable simulators.** For both the deterministic SIR model (a) and probabilistic Lotka-Volterra model (b), the Sliced-Wasserstein distance (lower is better) between observations and simulations as well as entropy of estimated sources (higher is better) for different choices of λ and without the entropy regularization (NA) are shown. Mean and standard deviation are computed over five runs.

Source estimation for the deterministic SIR model Our method is able to estimate a good source distribution for the deterministic SIR model: The Sliced-Wasserstein distance between simulations and observations is close to the minimum distance (Fig. 4a). In contrast to the benchmark tasks, estimating sources with entropy regularization does not lead to an increase in entropy for the SIR model, and the quality of the estimated source remains constant for various choices of λ . A possible explanation for this is that there is no degeneracy in the parameter space of the deterministic simulator, and there exists only one source distribution.

Source estimation on the probabilistic Lotka-Volterra model For the probabilistic Lotka-Volterra model, our method is also capable of estimating source distributions. As for the SIR model, the Sliced-Wasserstein distance between simulations and observations is close to the minimum distance (Fig. 4b). However, unlike the SIR model, estimating the source with entropy regularization yields a large increase in entropy compared to when not using the regularization. For the Lotka-Volterra model, our method yields a substantially higher entropy at no additional cost in terms of source quality.

The experiments on the SIR and Lotka-Volterra models show that our approach is able to scale to higher dimensional problems and can use gradients of complex simulators to estimate source distributions directly from a set of observations.

3.3 Estimating source distributions for the single-compartment Hodgkin-Huxley model

Single-compartment Hodgkin-Huxley simulator and summary statistics We use the simulator described in Bernaerts et al. [2] with 13 parameters. In data space, we use 5 commonly used summary statistics of the observed and simulated spike trains. These are the (logged) number of spikes, the mean of the resting potential, and the mean, variance and skewness of the voltage during external current stimulation. As the internal noise in the simulator has little effect on the summary statistics, we train a simple multi-layer perceptron as surrogate on 10^6 simulations. The parameters used to generate these training simulations were sampled from a uniform distribution that was used as the prior in Bernaerts et al. [2] (details on simulator, choice of surrogate and the surrogate training in Appendix A.8).

Finally, we estimate source distributions from a real-world dataset of electrophysiological recordings and a single compartment Hodgkin-Huxley simulator [43]. The dataset [46] consists of 1033 electrophysiological recordings from the mouse motor cortex. In general, parameter inference for Hodgkin-Huxley models can be challenging as models are often misspecified [50, 2].

Source estimation On visual inspection, simulations from the estimated source look similar to the original recordings (all observations spike at least once, spikes have similar magnitudes) and show none of the unrealistic properties (e.g., spiking before the stimulus is applied) that can be observed in some of the box uniform prior simulations (Fig. 5a). This match is also confirmed by the distribution of summary statistics, which match closely between simulations and observations (Fig. 5b). Furthermore, our method achieves good C2ST accuracy of 61% for different choices of λ (Fig. 5d), as well as a small Sliced-Wasserstein distance of 0.08 in the standardized space of summary statistics (Fig. 5e). While the source estimated without entropy regularization also achieves good

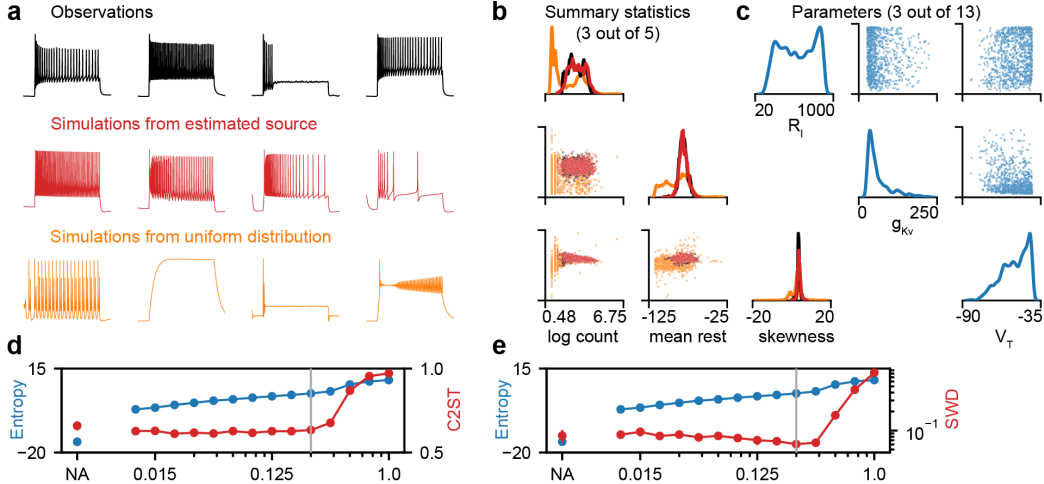


Figure 5: **Source estimation for the single-compartment Hodgkin-Huxley model.** (a) Example voltage traces of the real observations of the motor cortex dataset, simulations from the estimated source ($\lambda = 0.25$), and samples from the uniform distribution used to train the surrogate. (b) 1D and 2D marginals for three of the five summary statistics used to perform source estimation. (c) 1D and 2D marginal distributions of the estimated source for three of the 13 simulator parameters. (d and e) C2ST accuracy and Sliced-Wasserstein distance (lower is better) as well as entropy of estimated sources (higher is better) for different choices of λ including $\lambda = 0.25$ (gray line) and without entropy regularization (NA). Mean and standard deviation over five runs are shown.

fidelity, its entropy is significantly lower than any of the source distributions estimated with entropy regularization (Fig. 5d/e, example source distribution in Fig. 5c, full source in Appendix A.9).

Overall, these results demonstrate the importance of estimating source distributions using the entropy regularization, especially on real-world datasets: Estimating the source distribution without any entropy regularization can introduce severe bias, since the estimated source may ignore entire regions of the parameter space. In this example, the parameter space of the single-compartment Hodgkin-Huxley model is known to be highly degenerate, and a given observation can be generated by multiple parameter configurations [12, 35].

4 Related Work

Neural Empirical Bayes High-dimensional source distributions have been estimated through variational approximations to the empirical Bayes problem. Louppe et al. [30] trained a generative adversarial network (GAN) [18] q_ψ to approximate the source. The use of a discriminator to compute an implicit distance makes this approach purely sample-based as well. In order to find the optimal ψ^* of the true data-generating process, they augmented the adversarial loss with a small entropy penalty on the source q_ψ . This penalty encourages low entropy, point mass distributions, which is the *opposite* of our approach. Vandegar et al. [52] take an empirical Bayes approach, and use normalizing flows for both the variational approximation of the source and as a surrogate for the likelihood $p(x|\theta)$. This allows for direct regression on the marginal likelihood, as all likelihoods can be computed directly. Finally, the empirical Bayes problem is also known as “unfolding” in the particle physics literature [8], “population inference” in gravitational wave astronomy [49], and “population of models” in electrophysiology [26]. Approaches have been developed to identify the source distribution, including classical approaches that seek to increase the entropy of the learned sources [44].

Simulation-Based Inference The use of variational surrogates of the likelihood of a simulator with intractable likelihood is known as *Neural Likelihood Estimation* in the simulation-based inference (SBI) literature [54, 40, 32, 9]. In neural posterior estimation [39, 31, 19], an *amortized* posterior density estimate is learned, which can be applied to evaluate the posterior of a single observation

$x_i \in \mathcal{D}$, if a prior distribution $p(\theta)$ is already known. An intuitive but incorrect approach to source distribution estimation would be to take the *average posterior* distribution over the observations \mathcal{D} ,

$$G_n(\theta) = \frac{1}{n} \sum_{i=1}^n p(\theta|x_i). \quad (7)$$

The average posterior does not always (and typically does not) converge to a source distribution in the infinite data limit, as shown for simple examples in Appendix A.7. Intuitively, the average posterior becomes a worse approximation of a source distribution for simulators which have broader likelihoods. Instead, SBI can be seen as a downstream task of source distribution estimation; once a prior has been learned from the dataset of observations with source estimation, the posterior can be estimated for each new observation individually.

Generalized Bayesian Inference Another related field is Generalized Bayesian Inference (GBI) [5, 36]. Central to GBI is that in many inference applications, the exact Bayesian posterior distribution is not necessarily of interest, if one can find a distribution which can reproduce observations with high fidelity with respect to different distance metrics that can be chosen to target different features of the data. Similarly, Bayesian non-parametric methods [38, 34, 10] learn a posterior directly on the data space which can then be used to sample from a posterior distribution over the parameter space.

5 Summary and Discussion

In this work, we introduced Sourcerer as a method to estimate source distributions given datasets of observations. This is a common problem setting across a range of scientific and engineering disciplines. Our method has several advantages: first, we employ a maximum entropy approach, improving reproducibility of the learned source, as the maximum entropy source distribution is unique while the traditional source distribution estimation problem can be ill-posed. Second, our method allows for sample-based optimization. In contrast to previous likelihood-based approaches, this scales more readily to higher dimensional problems, and can be applied to simulators without a tractable likelihood. We demonstrated the performance of our approach across a diverse suite of tasks, including deterministic and probabilistic simulators, low- and high-dimensional observation spaces, and a contemporary scientific task of estimating a source distribution for the single-compartment Hodgkin-Huxley model from a dataset of electrophysiological recordings. Throughout our experiments, we have consistently found that our approach yields higher entropy sources without reducing the fidelity of simulations from the learned source.

Limitations A limitation of this work is the regularized regression approximation to the constrained optimization problem in Eq. 2. As a result, there are no guarantees on finding the maximum entropy source distribution. We leave the application of more sophisticated methods of constrained optimization, which could potentially provide more guarantees than our approach, to future work [14, 7]. Additionally, in this work, we used the Sliced-Wasserstein distance for the data-consistency term between simulations and observations. In practice, different distance metrics can lead to different estimated sources, depending on its sensitivity to different features. While our method is compatible with any sample-based differentiable distance metric between two distributions, there is still an onus on the practitioner to carefully select a reasonable distance metric for the data at hand. Similarly, there is a dependence on the terminal regularization strength λ , though as we demonstrate, our results are robust to a large range of λ . Finally, the method requires a differentiable simulator, which in practice may require the training of a surrogate model. While this is a common requirement for simulation-based methods, this could present a challenge for some applications.

6 Ethics Statement

We used data recorded from animal experiments in the mouse. The data we used were recorded for an independent study and have recently been made publicly available [46]. While our work has the potential to aid in scientific discovery across a broad range of disciplines, one could also imagine undesired uses.

Acknowledgements

This work was funded by the German Research Foundation (DFG) under Germany’s Excellence Strategy – EXC number 2064/1 – 390727645 and SFB 1233 ‘Robust Vision’ (276693517). This work was co-funded by the German Federal Ministry of Education and Research (BMBF): Tübingen AI Center, FKZ: 01IS18039A and the European Union (ERC, DeepCoMechTome, 101089288). Views and opinions expressed are however those of the author(s) only and do not necessarily reflect those of the European Union or the European Research Council. Neither the European Union nor the granting authority can be held responsible for them. JV is supported by the AI4Med-BW graduate program. JV and GM are members of the International Max Planck Research School for Intelligent Systems (IMPRS-IS). We would like to thank Jonas Beck, Sebastian Bischoff, Michael Deistler, Manuel Glöckler, Jaivardhan Kapoor, Auguste Schulz, and all members of Mackelab for feedback and discussion throughout the project.

References

- [1] Zafarali Ahmed, Nicolas Le Roux, Mohammad Norouzi, and Dale Schuurmans. Understanding the impact of entropy on policy optimization. In *International conference on machine learning*, 2019.
- [2] Yves Benaerts, Michael Deistler, Pedro J Goncalves, Jonas Beck, Marcel Stimberg, Federico Scala, Andreas S Tolias, Jakob H Macke, Dmitry Kobak, and Philipp Berens. Combined statistical-mechanistic modeling links ion channel genes to physiology of cortical neuron types. *bioRxiv*, 2023.
- [3] Thomas B. Berrett, Richard J. Samworth, and Ming Yuan. Efficient multivariate entropy estimation via k -nearest neighbour distances. *The Annals of Statistics*, 2019.
- [4] D.P. Bertsekas and W. Rheinboldt. *Constrained Optimization and Lagrange Multiplier Methods*. Computer science and applied mathematics. Elsevier Science, 2014.
- [5] Pier Giovanni Bissiri, Chris C Holmes, and Stephen G Walker. A general framework for updating belief distributions. *Journal of the Royal Statistical Society Series B: Statistical Methodology*, 2016.
- [6] Nicolas Bonneel, Julien Rabin, Gabriel Peyré, and Hanspeter Pfister. Sliced and Radon Wasserstein barycenters of measures. *Journal of Mathematical Imaging and Vision*, 2015.
- [7] E.K.P. Chong, W.S. Lu, and S.H. Zak. *An Introduction to Optimization: With Applications to Machine Learning*. Wiley, 2023.
- [8] G. Cowan. *Statistical Data Analysis*. Oxford science publications. Clarendon Press, 1998.
- [9] Kyle Cranmer, Johann Brehmer, and Gilles Louppe. The frontier of simulation-based inference. *Proceedings of the National Academy of Sciences*, 2019.
- [10] Charita Dellaporta, Jeremias Knoblauch, Theodoros Damoulas, and François-Xavier Briol. Robust Bayesian inference for simulator-based models via the MMD posterior bootstrap. In *International Conference on Artificial Intelligence and Statistics*. PMLR, 2022.
- [11] Laurent Dinh, Jascha Sohl-Dickstein, and Samy Bengio. Density estimation using Real NVP. In *International Conference on Learning Representations*, 2017.
- [12] Gerald M Edelman and Joseph A Gally. Degeneracy and complexity in biological systems. *Proceedings of the National Academy of Sciences*, 2001.
- [13] Bradley Efron and Carl Morris. Limiting the risk of Bayes and empirical Bayes estimators, part ii: The empirical Bayes case. *Journal of the American Statistical Association*, 1972.
- [14] Philip E. Gill, Walter Murray, and Margaret H. Wright. *Practical Optimization*. Society for Industrial and Applied Mathematics, 2019.

- [15] Manuel Glöckler, Michael Deistler, and Jakob H. Macke. Adversarial robustness of amortized Bayesian inference. In *International Conference on Machine Learning*, 2023.
- [16] Pedro J Gonçalves, Jan-Matthis Lueckmann, Michael Deistler, Marcel Nonnenmacher, Kaan Öcal, Giacomo Bassetto, Chaitanya Chintaluri, William F Podlaski, Sara A Haddad, Tim P Vogels, et al. Training deep neural density estimators to identify mechanistic models of neural dynamics. *Elife*, 2020.
- [17] I. J. Good. Maximum entropy for hypothesis formulation, especially for multidimensional contingency tables. *Annals of Mathematical Statistics*, 1963.
- [18] Ian Goodfellow, Jean Pouget-Abadie, Mehdi Mirza, Bing Xu, David Warde-Farley, Sherjil Ozair, Aaron Courville, and Yoshua Bengio. Generative adversarial nets. In *Advances in Neural Information Processing Systems*, 2014.
- [19] David S. Greenberg, Marcel Nonnenmacher, and Jakob H. Macke. Automatic posterior transformation for likelihood-free inference. In *International Conference on Machine Learning*, 2019.
- [20] Will Handley and Marius Millea. Maximum-entropy priors with derived parameters in a specified distribution. *Entropy*, 2018.
- [21] Edwin T. Jaynes. Prior probabilities. *IEEE Transactions on Systems Science and Cybernetics*, 1968.
- [22] Diederik P Kingma and Jimmy Ba. Adam: A method for stochastic optimization. *arXiv preprint arXiv:1412.6980*, 2014.
- [23] Soheil Kolouri, Kimia Nadjahi, Umut Simsekli, Roland Badeau, and Gustavo Rohde. Generalized Sliced Wasserstein distances. In *Advances in Neural Information Processing Systems*, 2019.
- [24] L. Kozachenko and N. Leonenko. A statistical estimate for the entropy of a random vector. *Problems of Information Transmission*, 1987.
- [25] H. W. Kuhn. The Hungarian method for the assignment problem. *Naval Research Logistics Quarterly*, 1955.
- [26] Brodie A. J. Lawson, Christopher C. Drovandi, Nicole Cusimano, Pamela Burrage, Blanca Rodriguez, and Kevin Burrage. Unlocking data sets by calibrating populations of models to data density: A study in atrial electrophysiology. *Science Advances*, 2018.
- [27] Tai Sing Lee and David Mumford. Hierarchical Bayesian inference in the visual cortex. *J. Opt. Soc. Am. A*, 2003.
- [28] Ning Leng, John A. Dawson, James A. Thomson, Victor Ruotti, Anna I. Rissman, Bart M. G. Smits, Jill D. Haag, Michael N. Gould, Ron M. Stewart, and Christina Kendzioriski. EBSeq: an empirical bayes hierarchical model for inference in RNA-seq experiments. *Bioinformatics*, 2013.
- [29] David Lopez-Paz and Maxime Oquab. Revisiting classifier two-sample tests. In *International Conference on Learning Representations*, 2017.
- [30] Gilles Louppe, Joeri Hermans, and Kyle Cranmer. Adversarial variational optimization of non-differentiable simulators. In Kamalika Chaudhuri and Masashi Sugiyama, editors, *International Conference on Artificial Intelligence and Statistics*, Proceedings of Machine Learning Research, 2019.
- [31] Jan-Matthis Lueckmann, Pedro J Gonçalves, Giacomo Bassetto, Kaan Öcal, Marcel Nonnenmacher, and Jakob H Macke. Flexible statistical inference for mechanistic models of neural dynamics. In *Advances in Neural Information Processing Systems*, 2017.

- [32] Jan-Matthis Lueckmann, Giacomo Bassetto, Theofanis Karaletsos, and Jakob H. Macke. Likelihood-free inference with emulator networks. In *Proceedings of The 1st Symposium on Advances in Approximate Bayesian Inference*, Proceedings of Machine Learning Research, 2019.
- [33] Jan-Matthis Lueckmann, Jan Boelts, David Greenberg, Pedro Goncalves, and Jakob Macke. Benchmarking simulation-based inference. In *International Conference on Artificial Intelligence and Statistics*, 2021.
- [34] Simon Lyddon, Chris C. Holmes, and Stephen G. Walker. General Bayesian updating and the loss-likelihood bootstrap. *Biometrika*, 2017.
- [35] Eve Marder and Adam L Taylor. Multiple models to capture the variability in biological neurons and networks. *Nature neuroscience*, 2011.
- [36] Takuo Matsubara, Jeremias Knoblauch, François-Xavier Briol, and Chris J Oates. Robust generalised Bayesian inference for intractable likelihoods. *Journal of the Royal Statistical Society Series B: Statistical Methodology*, 2022.
- [37] Kimia Nadjahi, Alain Durmus, Lénaïc Chizat, Soheil Kolouri, Shahin Shahrampour, and Umut Simsekli. Statistical and topological properties of sliced probability divergences. In *Advances in Neural Information Processing Systems*, 2020.
- [38] Peter Orbanz and Yee Whye Teh. Bayesian nonparametric models. *Encyclopedia of Machine Learning*, 2010.
- [39] George Papamakarios and Iain Murray. Fast ϵ -free inference of simulation models with Bayesian conditional density estimation. In *Advances in Neural Information Processing Systems*, 2016.
- [40] George Papamakarios, David C. Sterratt, and Iain Murray. Sequential neural likelihood: Fast likelihood-free inference with autoregressive flows. In *International Conference on Artificial Intelligence and Statistics*, 2018.
- [41] Georg Pichler, Pierre Colombo, Malik Boudiaf, Günther Koliander, and Pablo Piantanida. A differential entropy estimator for training neural networks. In *International Conference on Machine Learning*, 2022.
- [42] John Platt and Alan Barr. Constrained differential optimization. In *Neural Information Processing Systems*, 1987.
- [43] Martin Pospischil, Maria Toledo-Rodriguez, Cyril Monier, Zuzanna Piwkowska, Thierry Bal, Yves Frégnac, Henry Markram, and Alain Destexhe. Minimal Hodgkin–Huxley type models for different classes of cortical and thalamic neurons. *Biological cybernetics*, 2008.
- [44] Marcel Reginatto, Paul Goldhagen, and Sonja Neumann. Spectrum unfolding, sensitivity analysis and propagation of uncertainties with the maximum entropy deconvolution code MAXED. *Nuclear Instruments and Methods in Physics Research Section A: Accelerators, Spectrometers, Detectors and Associated Equipment*, 2002.
- [45] Herbert E. Robbins. An empirical bayes approach to statistics. In *Breakthroughs in Statistics: Foundations and basic theory*, 1956.
- [46] Federico Scala, Dmitry Kobak, Matteo Bernabucci, Yves Bernaerts, Cathryn René Cadwell, Jesus Ramon Castro, Leonard Hartmanis, Xiaolong Jiang, Sophie Laturus, Elanine Miranda, et al. Phenotypic variation of transcriptomic cell types in mouse motor cortex. *Nature*, 2021.
- [47] Scott A Sisson, Yanan Fan, and Mark M Tanaka. Sequential monte carlo without likelihoods. *Proceedings of the National Academy of Sciences*, 2007.
- [48] Alvaro Tejero-Cantero, Jan Boelts, Michael Deistler, Jan-Matthis Lueckmann, Conor Durkan, Pedro J. Goncalves, David S. Greenberg, and Jakob H. Macke. sbi: A toolkit for simulation-based inference. *Journal of Open Source Software*, 2020.

- [49] Eric Thrane and Colm Talbot. An introduction to Bayesian inference in gravitational-wave astronomy: Parameter estimation, model selection, and hierarchical models. *Publications of the Astronomical Society of Australia*, 2019.
- [50] Nicholas Tolley, Pedro LC Rodrigues, Alexandre Gramfort, and Stephanie Jones. Methods and considerations for estimating parameters in biophysically detailed neural models with simulation based inference. *bioRxiv*, 2023.
- [51] Pravin M. Vaidya. An $O(n \log n)$ algorithm for the all-nearest-neighbors problem. *Discrete & Computational Geometry*, 1989.
- [52] Maxime Vandegar, Michael Kagan, Antoine Wehenkel, and Gilles Louppe. Neural empirical Bayes: Source distribution estimation and its applications to simulation-based inference. In *International Conference on Artificial Intelligence and Statistics*, 2020.
- [53] Yixin Wang, Andrew C. Miller, and David M. Blei. Comment: Variational Autoencoders as Empirical Bayes. *Statistical Science*, 2019.
- [54] Simon N. Wood. Statistical inference for noisy nonlinear ecological dynamic systems. *Nature*, 2010.

A Appendix

A.1 Simulators and sources

Here we provide a definition of the four benchmark tasks Two Moons (TM), Inverse Kinematics (IK), Simple Likelihood Complex Posterior (SLCP) and Gaussian Mixture (GM), as well as the two high-dimensional simulators, the SIR and Lotka-Volterra model. We also describe the original source distribution used to generate the synthetic observations, and the bounds of the reference uniform distribution on the parameters.

A.1.1 Two moons simulator

Dimensionality	$x \in \mathbb{R}^2, \theta \in \mathbb{R}^2$
Bounded domain	$[-5, 5]^2$
Original source	$\theta \sim \mathcal{U}([-1, 1]^2)$
Simulator	$x \theta = \begin{bmatrix} r \cos(\alpha) + 0.25 \\ r \sin(\alpha) \end{bmatrix} + \begin{bmatrix} - \theta_1 + \theta_2 /\sqrt{2} \\ (-\theta_1 + \theta_2)/\sqrt{2} \end{bmatrix}$, where $\alpha \sim U(-\pi/2, \pi/2)$, $r \sim \mathcal{N}(0.1, 0.01^2)$.
References	Vandegar et al. [52], Lueckmann et al. [33]

A.1.2 Inverse Kinematics simulator

Dimensionality	$x \in \mathbb{R}^2, \theta \in \mathbb{R}^4$
Bounded domain	$[-\pi, \pi]^4$
Original source	$\theta \sim \mathcal{N}(0, \text{Diag}(\frac{1}{2}, \frac{1}{4}, \frac{1}{4}, \frac{1}{4}))$
Simulator	$x_1 = \theta_1 + l_1 \sin(\theta_2 + \epsilon) + l_2 \sin(\theta_2 + \theta_3 + \epsilon) + l_3 \sin(\theta_2 + \theta_3 + \theta_4 + \epsilon)$, $x_2 = l_1 \cos(\theta_2 + \epsilon) + l_2 \cos(\theta_2 + \theta_3 + \epsilon) + l_3 \cos(\theta_2 + \theta_3 + \theta_4 + \epsilon)$, where $l_1 = l_2 = 0.5$, $l_3 = 1.0$ and $\epsilon \sim \mathcal{N}(0, 0.00017^2)$.
References	Vandegar et al. [52]

A.1.3 SLCP simulator

Dimensionality	$x \in \mathbb{R}^8, \theta \in \mathbb{R}^5$
Bounded domain	$[-5, 5]^5$
Original source	$\theta \sim \mathcal{U}([-3, 3]^5)$
Simulator	$x \theta = (x_1, \dots, x_4), x_i \sim \mathcal{N}(m_\theta, S_\theta)$, where $m_\theta = \begin{bmatrix} \theta_1 \\ \theta_2 \end{bmatrix}$, $S_\theta = \begin{bmatrix} s_1^2 & \rho s_1 s_2 \\ \rho s_1 s_2 & s_2^2 \end{bmatrix}$, $s_1 = \theta_3^2$, $s_2 = \theta_4^2$, $\rho = \tanh \theta_5$.
References	Vandegar et al. [52], Lueckmann et al. [33]

A.1.4 Gaussian mixture simulator

Dimensionality	$x \in \mathbb{R}^2, \theta \in \mathbb{R}^2$
Bounded domain	$[-5, 5]^2$
Original source	$\theta \sim \mathcal{U}([0.5, 1]^2)$
Simulator	$x \theta \sim 0.5\mathcal{N}(x \theta, I) + 0.5\mathcal{N}(x \theta, 0.01 \cdot I)$.
References	Sisson et al. [47]

A.1.5 SIR model

Dimensionality	$x \in \mathbb{R}^{50}, \theta \in \mathbb{R}^2$
Bounded domain	$[0.001, 3]^2$
Original source	$\beta \sim \text{LogNormal}(\log(0.4), 0.5)$ $\gamma \sim \text{LogNormal}(\log(0.125), 0.2)$
Simulator	$x \theta = (x_1, \dots, x_{50})$, where $x_i = I_i/N$ equally spaced and I is simulated from $\frac{dS}{dt} = -\beta \frac{SI}{N}$, $\frac{dI}{dt} = \beta \frac{SI}{N} - \gamma I$, $\frac{dR}{dt} = \gamma I$ with initial values $S = N - 1$, $I = 1$, $R = 0$ and $N = 10^6$.
References	Lueckmann et al. [33]

A.1.6 Lotka-Volterra model

Dimensionality	$x \in \mathbb{R}^{100}, \theta \in \mathbb{R}^4$
Bounded domain	$[0.1, 3]^4$
Original source	$\theta' \sim \mathcal{N}(0, 0.5^2)^4$, pushed through $\theta = f(\theta') = \exp(\sigma(\theta'))$, where σ is the sigmoid function.
Simulator	$x \theta = (x_1^X, \dots, x_{50}^X, x_1^Y, \dots, x_{50}^Y)$, where $x_i^X \sim \mathcal{N}(X, 0.05^2)$, $x_i^Y \sim \mathcal{N}(Y, 0.05^2)$ equally spaced, and X, Y are simulated from $\frac{dX}{dt} = \alpha X - \beta XY$, $\frac{dY}{dt} = -\gamma Y + \delta XY$ with initial values $X = Y = 1$.
References	Glöckler et al. [15]

A.2 Pseudocode and details on source estimation for benchmark tasks

Pseudocode for Sourcerer is provided in Algorithm 1.

For both the benchmark tasks and high dimensional simulators, sources were estimated from 10000 synthetic observations that were generated by simulating samples from an original previously defined source.

For the benchmark tasks, we used $T = 500$ linear decay steps from $\lambda_{t=0}$ to $\lambda_{t=T} = \lambda$ and optimized the source model using the Adam optimizer with a learning rate of 10^{-4} and weight decay of 10^{-5} . The two high dimensional simulators were optimized with a higher learning rate of 10^{-3} and $T = 50$ linear decay steps. In both cases, early stopping was performed when the overall loss in Eq. (4) did not improve over a set number of training iterations.

As a baseline, we compare to Neural Empirical Bayes (NEB) as described in Vandegar et al. [52]. Specifically, we use the biased estimator with 1024 samples per observation (\mathcal{L}_{1024}), which are used to compute the Monte Carlo integral. Unlike our Sliced-Wasserstein-based approach, NEB does not operate on the whole dataset of observations directly but attempts to maximize the marginal likelihood per observation and thus uses part of the observations as a validation set. To ensure a fair comparison, we increased the number of observations to 11112 for all NEB experiments, which results in a training dataset of 10000 observations when using 10% as a validation set. For training, we again used the Adam optimizer (learning rate 10^{-4} , weight decay 10^{-5} , training batch size 128).

Algorithm 1: Sourcerer

Inputs: Source model q_ϕ constrained on the bounded domain B_Θ , observed dataset $\mathcal{D} = \{x_1, \dots, x_n\} \sim p_o(x)$, differentiable model $p(x|\theta)$ to draw samples from (simulator or surrogate), number of samples m to estimate entropy, regularization schedule $\lambda_{t=1}, \dots, \lambda_{t=T}$.
Outputs: Trained source model $q_\phi(\theta)$.

```

t ← 0;
while not converged do
     $\theta_1, \dots, \theta_n \sim q_\phi(\theta)$ ;           # sample parameters for pushforward
     $x'_i \sim p(x|\theta_i)$ ;                 # sample pushforward
     $\theta'_1, \dots, \theta'_m \sim q_\phi(\theta)$ ; # sample parameters for entropy estimation
     $\lambda \leftarrow \lambda_{t=t}$  if  $t \leq T$  else  $\lambda_{t=T}$ ; # schedule lambda
     $\mathcal{L} \leftarrow \lambda H(\{\theta'_1, \dots, \theta'_m\}) + (1 - \lambda) D(\{x_1, \dots, x_n\}, \{x'_1, \dots, x'_n\})$ ; # compute loss
     $\phi \leftarrow \phi - \text{Adam}(\nabla_\phi \mathcal{L})$ ; # update source model
    t ← t + 1
return  $q_\phi$ 

```

A.3 Source model

Throughout all our experiments, we use neural samplers as the source models [52]. The sampler architecture is a three-layer multi-layer perceptron with dimension of 100, ReLU activations and batch normalization as our source model. Samples are generated by drawing a sample $s \sim \mathcal{N}(0, I)$ from the standard multivariate Gaussian and then (non-linearly) transforming s with the neural network.

A.4 Surrogates for the benchmark tasks

We follow Vandegar et al. [52] and train RealNVP flows [11] as surrogates for the four benchmark tasks. For all benchmark tasks, the RealNVP surrogates have a flow length of 8 layers with a hidden dimension of 50.

Surrogates were trained using the Adam optimizer [22] on 15000 samples and simulator evaluations from the uniform distribution over the bounded domain (learning rate 10^{-4} , weight decay $5 \cdot 10^{-5}$, training batch size 256). In addition, 20% of the data was used for validation.

A.5 Kozachenko-Leonenko entropy estimator

Our use of neural samplers requires us to use a sample-based estimate of (differential) entropy, since no tractable likelihood is available (see Sec. 2.5).

We use the Kozachenko-Leonenko estimator [24, 3] for a set of samples $\{\theta_i\}_{i=1}^n$ from a distribution $p(\theta) \in P(\Theta)$, given by

$$H(q_\phi) \approx \frac{d}{m} \left[\sum_{i=1}^n \log(d_i) \right] - g(k) + g(n) + \log(V_d), \quad (8)$$

where d_i is the distance of θ_i from its k -th nearest neighbor in $\{\theta_j\}_{j \neq i}$, d is the dimensionality of Θ , m is the number of non-zero values of d_i , g is the digamma function, and V_d is the volume of the unit ball using the same distance measure as used to compute the distances d_i .

The Kozachenko-Leonenko estimator is differentiable and can be used for gradient-based optimization. The all-pairs nearest neighbor problem can be efficiently solved in $\mathcal{O}(n \log n)$ [51]. In practice, we find all nearest neighbors by computing all pairwise distances on a fixed number of samples. Throughout all experiments, 512 source distribution samples were used to estimate the entropy during training.

A.6 Uniqueness of maximum entropy source distribution

Here, we prove the uniqueness of the maximum entropy source distribution (Proposition 2.1). First, however, we demonstrate for a simple example that the source distribution without the maximum entropy condition is not unique.

Example of non-uniqueness Consider the (deterministic) simulator $x = f(\theta) = |\theta|$. Further assume that our observed distribution is the uniform distribution $p(x) = \mathcal{U}(x; a, b)$, where $0 < a < b$. Due the symmetry of f , the source distribution $p(\theta)$ for the observed distribution $p(x)$ is not unique. Any convex combination of form $\alpha u_1(\theta) + (1 - \alpha)u_2$, where $u_1(\theta) = \mathcal{U}(\theta; -b, -a)$ and $u_2(\theta) = \mathcal{U}(\theta; a, b)$ and $\alpha \in [0, 1]$ provides a source distribution. The maximum entropy source distribution is unique and is attained if both distributions are weighted equally with $\alpha = 0.5$.

Proof of Proposition 2.1 First, let us state Proposition 2.1 in full:

Let $\Theta \subset \mathbb{R}^{d_\Theta}$ and $\mathcal{X} \subset \mathbb{R}^{d_{\mathcal{X}}}$ be the parameter and observation spaces, respectively. Suppose that Θ is compact. Let $\mathcal{P}(\Theta) \subset L^1(\Theta)$ and $\mathcal{P}(\mathcal{X}) \subset L^1(\mathcal{X})$ be the set of probability measures on Θ and \mathcal{X} respectively. Let $Q = \{q | q^\# = p_o \text{ almost everywhere} \} \subset \mathcal{P}(\Theta)$ be the set of source distributions for a given likelihood $p(x|\theta)$ and data distribution $p_o \in \mathcal{P}(\mathcal{X})$. Suppose that Q is non-empty and compact (in the L^1 norm topology). Then $q^* = \arg \max_{q \in Q} H(q)$ exists and is unique.

We require two results to prove that the maximum entropy source distribution is unique. First, the set of source distributions Q is a convex set, i.e., convex combinations of source distributions are also source distributions. Second, (differential) entropy is strictly concave.

Let q_1 and q_2 be two distinct source distributions, then their convex combination $q = \alpha q_1 + (1 - \alpha)q_2$, $\alpha \in [0, 1]$ is a valid probability distribution supported on both of the supports of q_1 and q_2 .

Sources distributions are closed under convex combination: q is also a source distribution, since

$$\begin{aligned}
q^\#(x) &= \int p(x|\theta) \cdot (\alpha q_1(\theta) + (1 - \alpha)q_2(\theta))d\theta \\
&= \alpha \int p(x|\theta)q_1(\theta)d\theta + (1 - \alpha) \int p(x|\theta)q_2(\theta)d\theta \\
&= \alpha p_o(x) + (1 - \alpha)p_o(x) = p_o(x).
\end{aligned} \tag{9}$$

Entropy is (strictly) concave: by the compactness assumption on Θ , the (differential) entropy of all $q \in P(\Theta)$ is bounded above (by the entropy of the uniform distribution on Θ), and so in particular the entropy is finite. The entropy of q satisfies

$$\begin{aligned}
H(q) &= - \int (\alpha q_1(\theta) + (1 - \alpha)q_2(\theta)) \cdot \log(\alpha q_1(\theta) + (1 - \alpha)q_2(\theta))d\theta \\
&\geq - \int [\alpha q_1(\theta) \log(q_1(\theta)) + (1 - \alpha)q_2(\theta) \log(q_2(\theta))]d\theta \\
&= \alpha H(q_1) + (1 - \alpha)H(q_2),
\end{aligned} \tag{10}$$

where we used the fact that the function $f(x) = x \log x$ is convex on $[0, \infty)$, and hence $-f$ is concave. Furthermore, $f(x)$ is strictly convex on $[0, \infty)$, so for any $\theta \in \Theta$, the equality of the integrands

$$\alpha q_1(\theta) + (1 - \alpha)q_2(\theta) \log(\alpha q_1(\theta) + (1 - \alpha)q_2(\theta)) = \alpha q_1(\theta) \log(q_1(\theta)) + (1 - \alpha)q_2(\theta) \log(q_2(\theta)) \tag{11}$$

holds if and only if $\alpha \in \{0, 1\}$ or $q_1(\theta) = q_2(\theta)$. Since q_1 and q_2 are assumed distinct, that is, it holds $q_1(\theta) \neq q_2(\theta)$ on a positive measure set, the integral equality in Eq. (10) only holds if $\alpha \in \{0, 1\}$, and thus entropy is strictly concave.

As Q is assumed compact, and the entropy is bounded above on Q , then the entropy achieves its supremum on Q . That is, there is a q^* such that $H(q^*) = \sup_{q \in Q} H(q)$ exists. Since we have shown the set Q is convex and the entropy is strictly concave, q^* is unique (up to L^1 -null sets).

□

A.7 Examples related to the average posterior distribution

In general, the average posterior distribution is not a source distribution. The average posterior distribution is defined in Eq. (7). The infinite data limit is given by $G_n(\theta) \xrightarrow{n \rightarrow \infty} G(\theta) = \int p(\theta|x)p_o(x)dx$. Here, we provide two examples, one based on coin flips, and one based on a Gaussian bimodal likelihood to illustrate this point.

Coin-flip example Consider the classical coin flip example, where the probability of heads (H) follows a Bernoulli distribution with parameter θ . The source distribution estimation problem for this setting would consist of the outcomes of flipping n distinct coins, with potentially different values θ_i .

Proposition A.1. *Suppose we have a Beta prior distribution on the Bernoulli parameter $\theta \sim \text{Beta}(\alpha, \beta)$ with parameters $\alpha = \beta = 1$, and that the empirical measurements consist of 70% heads, i.e.:*

$$p_o(x) = \begin{cases} 0.7 & x = H \\ 0.3 & x = T \end{cases}$$

Then the average posterior $G(\theta) = \int p(\theta|x)p_o(x)dx$ is not a source distribution for $p_o(x)$.

Proof: Since the Beta distribution is the conjugate prior for the Bernoulli likelihood, the single-observation posteriors are known to be $p(\theta|x = H) = \text{Beta}(2, 1)$ and $p(\theta|x = T) = \text{Beta}(1, 2)$. Hence, the average posterior is

$$G(\theta) = 0.3 \cdot \text{Beta}(1, 2) + 0.7 \cdot \text{Beta}(2, 1). \tag{12}$$

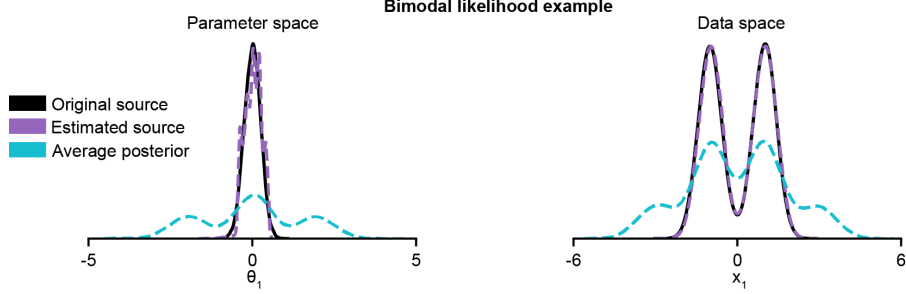


Figure 6: Failure of the average posterior as a source distribution for the bimodal likelihood example. Each of the individual posteriors is bimodal, resulting in an average posterior with 3 modes (left), the secondary modes produce observations which are not observed in the data distribution when pushed through the likelihood (right), and should not be part of the source distribution.

However, the ratio of heads observed when pushing this distribution through the Bernoulli simulator is

$$\begin{aligned}
 G^\#(x = \mathbf{H}) &= \int_0^1 \theta [0.3 \cdot \text{Beta}(\theta; 1, 2) + 0.7 \cdot \text{Beta}(\theta; 2, 1)] d\theta \\
 &= \int_0^1 \theta \left[0.3 \frac{1-\theta}{B(1, 2)} + 0.7 \frac{\theta}{B(2, 1)} \right] d\theta \\
 &= 2 \int_0^1 [0.3\theta(1-\theta) + 0.7\theta^2] d\theta \\
 &= 0.3\theta^2 + \frac{2}{3}0.4\theta^3 \Big|_0^1 \approx 0.567 \neq 0.7,
 \end{aligned} \tag{13}$$

where we have used the fact that the Beta function takes the values $B(1, 2) = B(2, 1) = 1/2$. Therefore, the pushforward of the average posterior distribution does not recover the correct ratio of heads, and so it is not a source distribution.

Gaussian bimodal example As another illustrative example to show the differences between average posterior and estimated source, we consider a one-dimensional, bimodal Gaussian likelihood given by $x|\theta \sim 0.5\mathcal{N}(x|\theta - 1, 0.3^2) + 0.5\mathcal{N}(x|\theta + 1, 0.3^2)$ and the source $\mathcal{N}(\theta|0, 0.25^2)$. We use the SBI package [48] and perform neural posterior estimation with the uniform prior $\theta \sim \mathcal{U}([-5, 5])$ to obtain the average posterior and compare it to the source estimated with our approach.

While the estimated source matches the original source closely, the average posterior is visibly different and substantially broader (Fig. 6). As expected, this difference persists when sampling from the average posterior and estimated source to simulate from the likelihood. The pushforward distributions in data space of the original and estimated source match, while the one of the average posterior is again substantially different (Fig. 6).

Additional average posteriors (in comparison to original and estimated source distributions) for the Two Moons and Gaussian mixture are shown in Fig. 9.

A.8 Details on source estimation for the single-compartment Hodgkin-Huxley model

We use the simulators as described in Bernaerts et al. [2] for our source estimation. This work provides a uniform prior over a specified box domain, which we use as the reference distribution for source estimation. Since the simulator parameters live on different orders of magnitude, we transform the original m -dimensional box domain to the $[-1, 1]^m$ cube. Note that this transformation does not affect the maximum entropy source distribution. This is because this scaling results in a constant term added to the (differential) entropy. More specifically, for a random variable X (associated with its probability density $p(x)$), the (differential) entropy of X scaled by a (diagonal) scaling matrix D and shifted by a vector c is given by

$$H(DX + c) = H(X) + \log(\det D). \tag{14}$$

The surrogate is trained on one million parameter-simulation pairs produced by sampling parameters from the uniform distribution and simulating with the sampled parameters. We do not use the simulated traces directly, but instead compute 5 commonly used summary statistics [2, 16]. These are the number of spikes k transformed by a $\log(k + 3)$ transformation (ensuring it is defined in the case of $k = 0$), the mean of the resting potential, and the first three moments (mean, variance, and skewness) of the voltage during the stimulation.

As our surrogate, we choose a deterministic multi-layer perceptron, because we found that the internal noise has almost no noticeable effect on the summary statistics, so that the likelihood $p(x|\theta)$ is essentially a point function. We are able to make this choice because the sample based nature of our source distribution estimation approach is less sensitive to sharp likelihood functions, whereas likelihood-based approaches could struggle with such problems.

The multi-layer perceptron surrogate has 3 layers with a hidden dimension of 256. ReLU activations and batch normalization were used. Training of the MLP was done with Adam (learning rate $5 \cdot 10^{-4}$, weight decay 10^{-5} , training batch size 4096). Again, 20% of the data were used for validation.

A.9 Supplementary figures

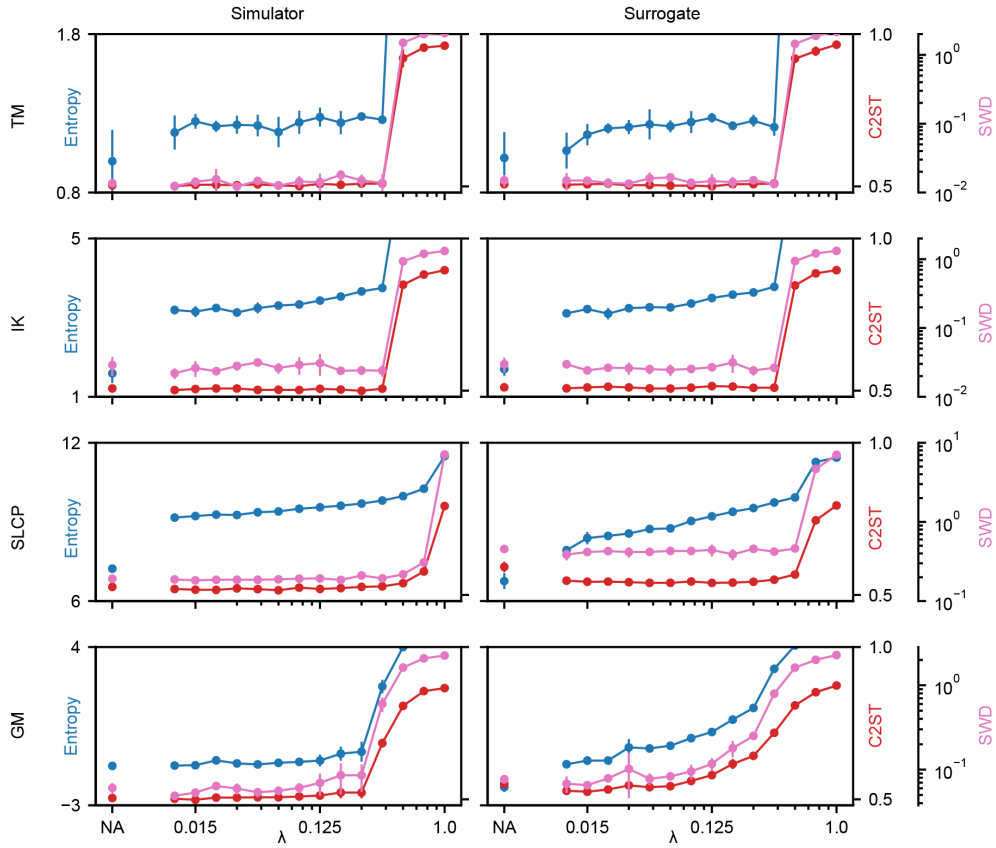


Figure 7: Extended results for source distribution estimation on the benchmark tasks (Fig. 3) for different choices of λ . In addition to the C2ST accuracy and entropy, here the Sliced-Wasserstein distance (SWD) between the observations and the pushforward distribution of the estimated source is shown. Mean and standard deviation were computed over five runs.

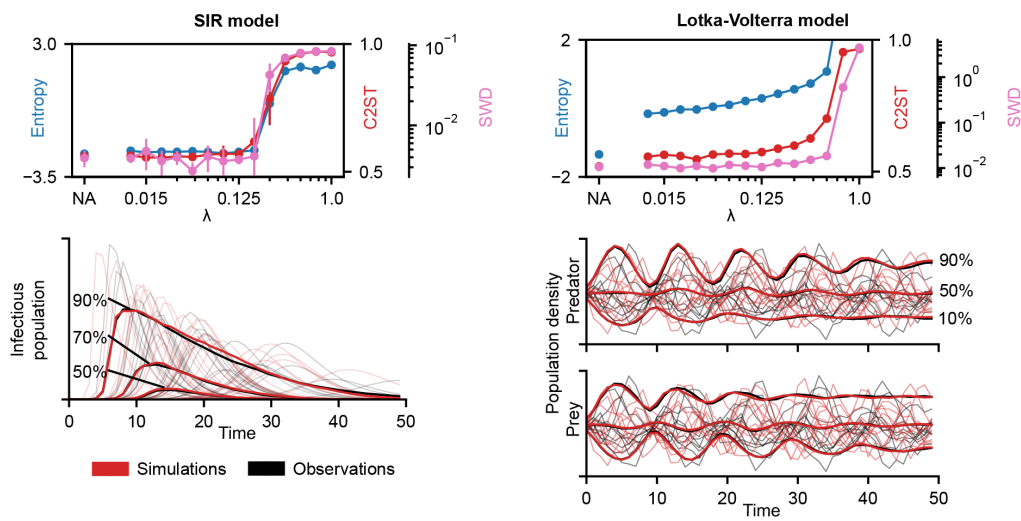


Figure 8: Extended results for source distribution estimation on the differentiable SIR and Lotka-Volterra models (Fig. 4). In addition to the Sliced-Wasserstein distance (SWD), the C2ST accuracy between the observations and the pushforward distribution of the the estimated source is shown. Despite the high-dimensional data space of the simulators (50 and 100 dimensions), the estimated sources achieve a good C2ST accuracy (below 60%) for various choices of λ . Mean and standard deviation were computed over five runs. Additionally, percentile values of all samples computed per time point between simulations (simulated with parameters from the estimated source) and observations (simulated with parameters from the original source) closely match.

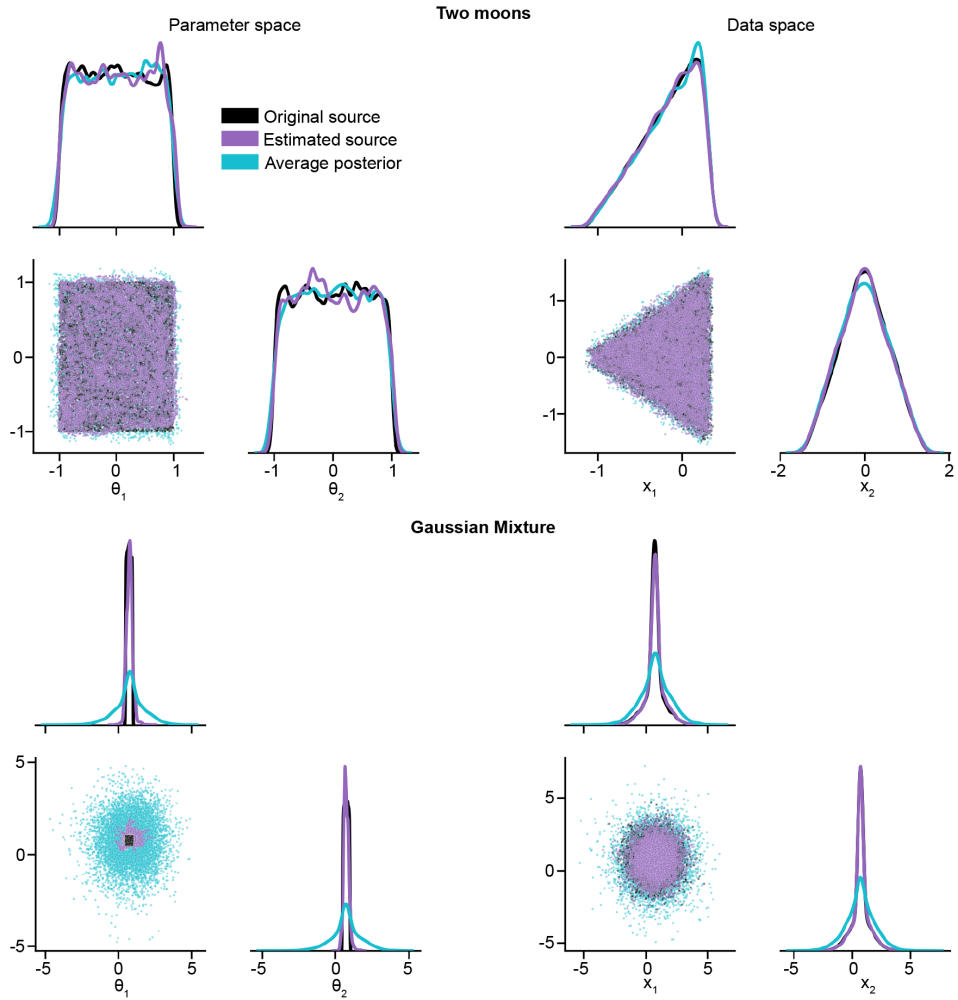


Figure 9: Original and estimated sources distributions as well as average posterior distribution for Two Moons and Gaussian Mixture simulator with uniform prior $\theta \sim \mathcal{U}([-5, 5]^2)$. For simulators for which the likelihood is unimodal and narrow (‘near-deterministic’), such as in the Two Moons simulator, the average posterior can be a good approximation of a source distribution. However, for simulators where the likelihood is broader, such as the Gaussian Mixture simulator, the average posterior is too broad, and does not reproduce the data distribution p_o well, when compared to estimates of source distributions.

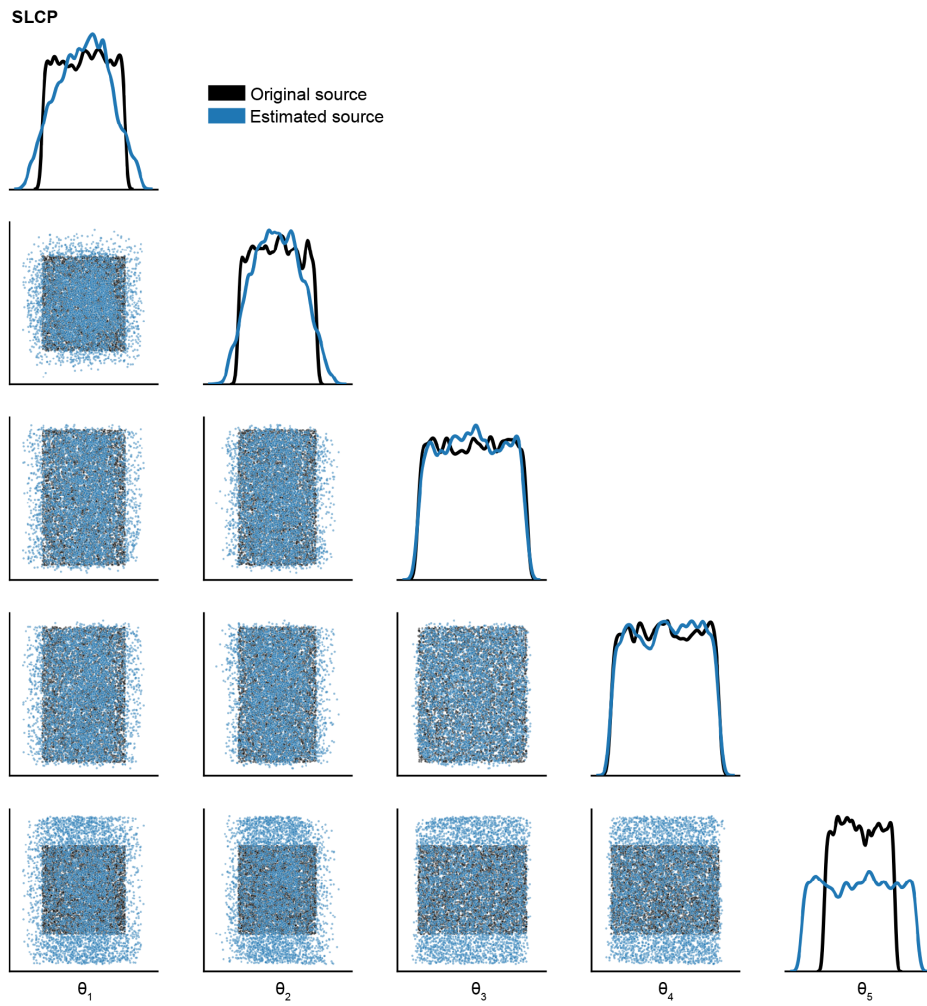


Figure 10: Original and estimated source distributions for the benchmark SLCP simulator. The estimated source has higher entropy than the original source.

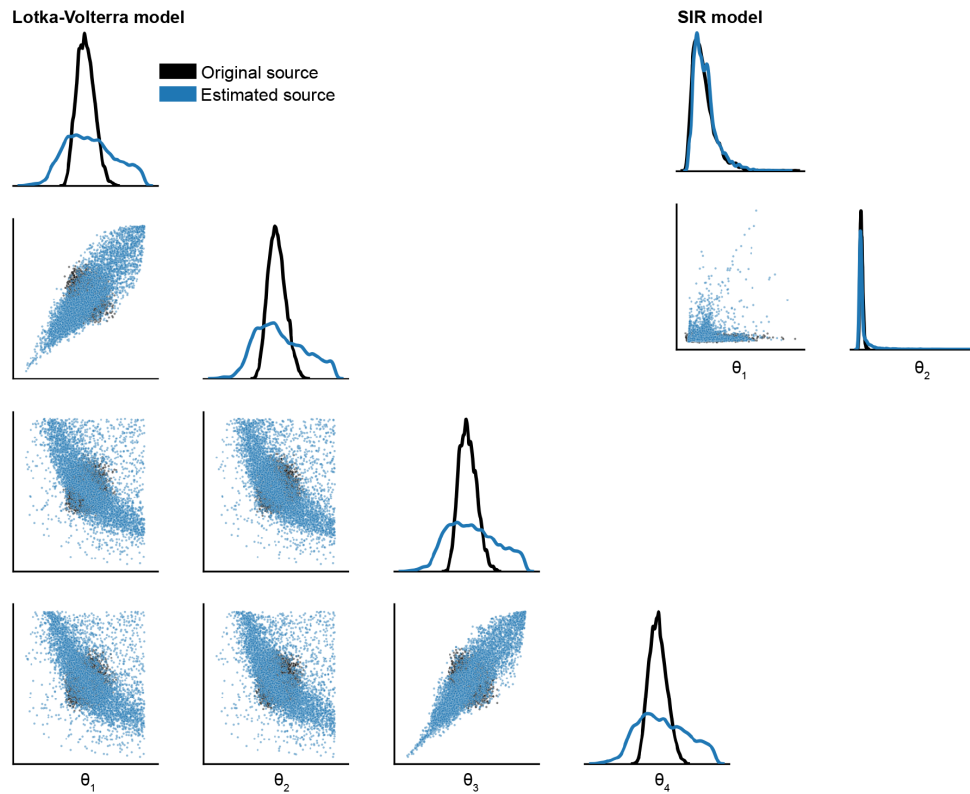


Figure 11: Original and estimated source distributions for the SIR and Lotka-Volterra model. For the Lotka-Volterra model, the estimated source has higher entropy than the original source.

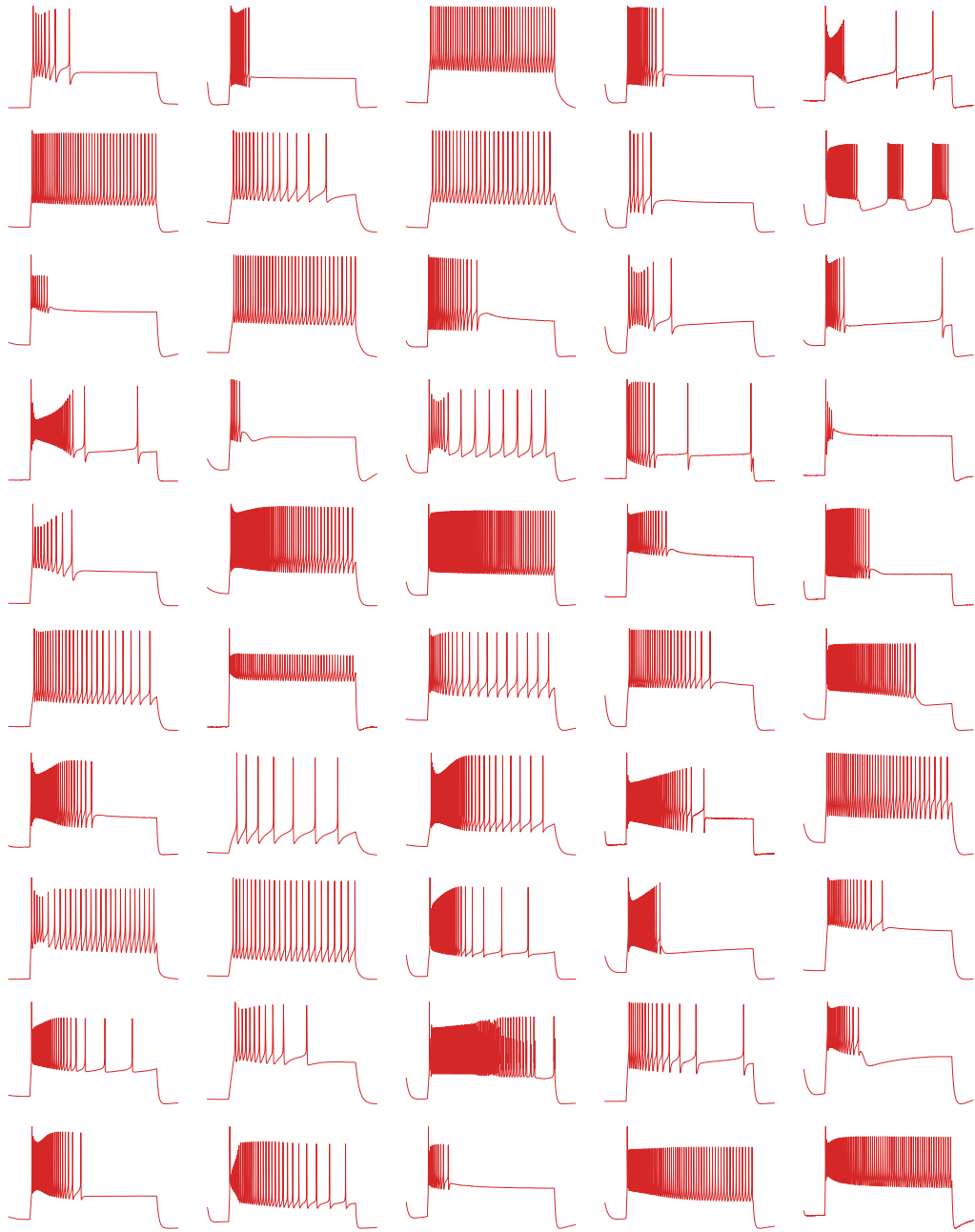


Figure 12: 50 random example traces produced by sampling from the estimated source and simulating with the Hodgkin-Huxley model.

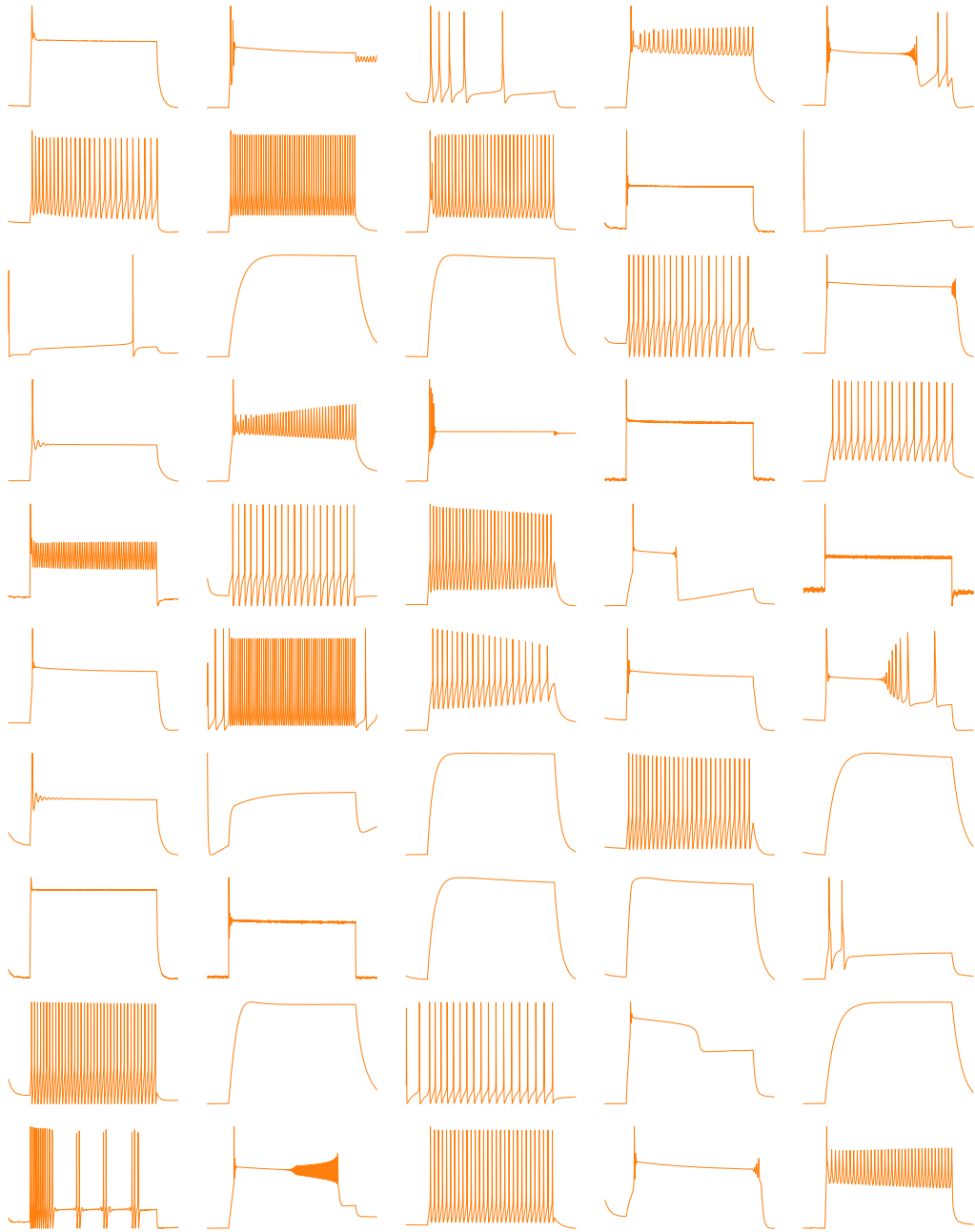


Figure 13: 50 random example traces produced by sampling from the uniform distribution over the box domain and simulating with the Hodgkin-Huxley model.

Hodgkin-Huxley model

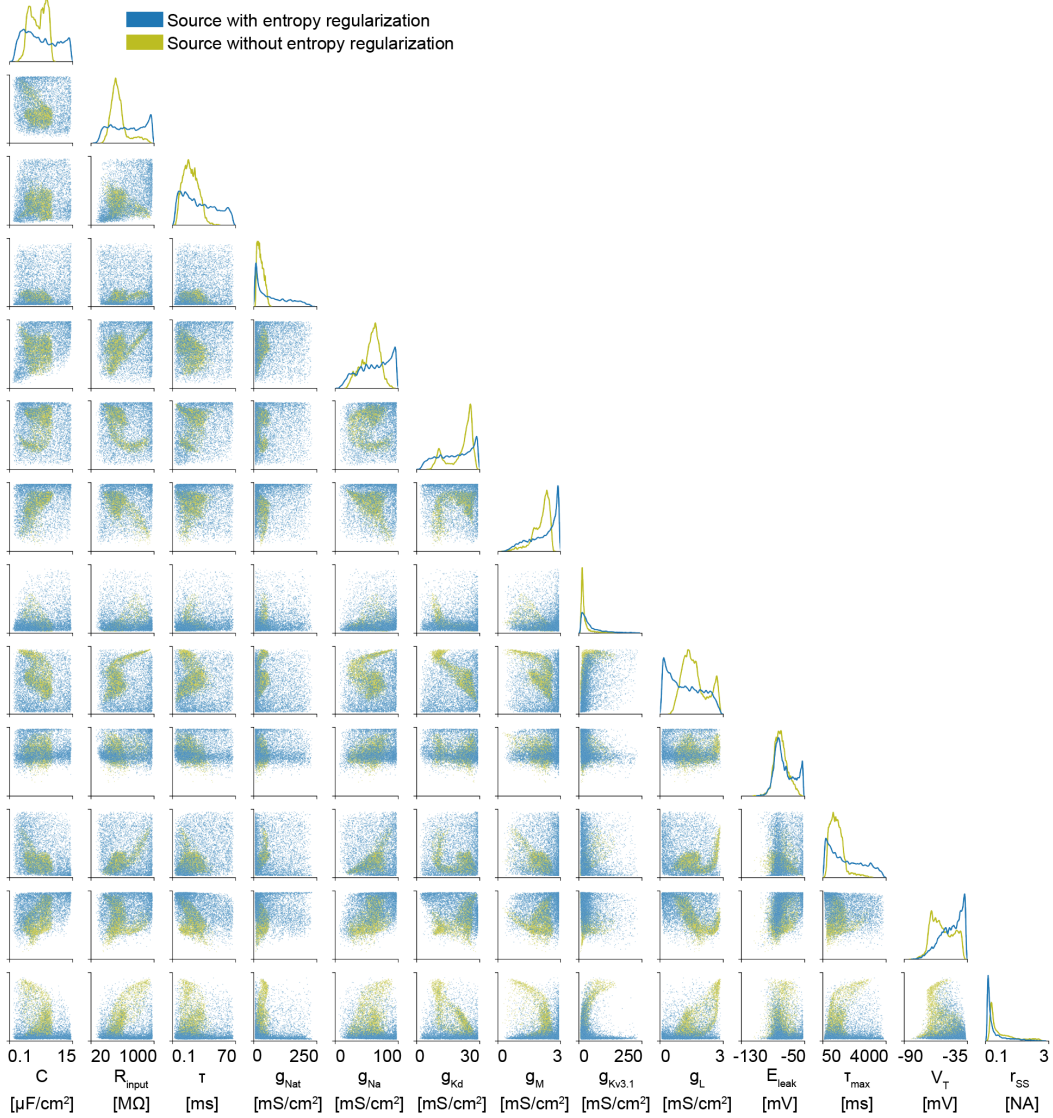


Figure 14: Estimated sources using for Hodgkin-Huxley task with the entropy regularization ($\lambda = 0.25$) and without the entropy regularization. Without, many viable parameter settings are missed, which would have significant downstream effects if the learned source distribution is used as a prior distribution for inference tasks.